Aqueous Zn Batteries Hot Paper

Zitierweise: Angew. Chem. Int. Ed. 2023, 62, e202300705
Internationale Ausgabe: doi.org/10.1002/anie.202300705
Deutsche Ausgabe: doi.org/10.1002/ange.202300705

Dynamically Resettable Electrode-Electrolyte Interface through Supramolecular Sol-Gel Transition Electrolyte for Flexible Zinc Batteries

Pengzhou Li[+], Meng Liao[+], Shuquan Cui, Jiaxin Li, Lei Ye, Yibei Yang, Chuang Wang, Bingjie Wang, and Huisheng Peng**

Abstract: Flexible batteries based on gel electrolytes with high safety are promising power solutions for wearable electronics but suffer from vulnerable electrode-electrolyte interfaces especially upon complex deformations, leading to irreversible capacity loss or even battery collapse. Here, a supramolecular sol-gel transition electrolyte (SGTE) that can dynamically accommodate deformations and repair electrode-electrolyte interfaces through its controllable rewetting at low temperatures is designed. Mediated by the micellization of polypropylene oxide blocks in Pluronic and host-guest interactions between α-cyclodextrin (α-CD) and polyethylene oxide blocks, the high ionic conductivity and compatibility with various salts of SGTE afford resettable electrode-electrolyte interfaces and thus constructions of a series of highly durable, flexible aqueous zinc batteries. The design of this novel gel electrolyte provides new insights for the development of flexible batteries.

The rapid rise of wearable electronics calls for corresponding power sources with high flexibility and security. With inherent safety[1] and low price,[2] flexible aqueous batteries are deemed one of the most promising energy storage devices for wearable electronics.[3] Upon operations in wearable devices, flexible batteries inevitably undergo various complex deformations.[4] In this regard, it is vital to eliminate the leakage of liquid electrolytes under deformations and reduce the undesirable side reactions resulting from the distortion of electrodes upon cycling,[5] which undermines the safety and electrochemical performances.

Gel electrolytes with high ionic conductivity and low fluidity are ideal for flexible batteries regarding structural integrity and electrochemical performances.[6] However, there are still some limitations to the full implementation of existing gel electrolytes in flexible batteries. First, conventional gel electrolytes cannot infiltrate inner electrode materials and easily detach under external distortions.[7] Deterioration of slippage-induced interfacial contact will cause a non-uniform localized electric field and inhomogeneous metal ion deposition, leading to poor electrode-electrolyte interfaces, low utilization of active materials, vigorous growth of dendrites, and even complete battery failure.[8] Second, electrolyte salts will influence the solubility of polymer hosts according to the Hofmeister series, i.e., saline-out ions (e.g., SO_4^{2-}) are prior to precipitating polymers and only limited electrolyte salts can be dissolved.[9] Hence, it is essential while challenging to design a stable gel electrolyte-electrode interface for flexible batteries capable of dynamically repairing electrode defects and maintaining conformal contact with electrode materials.

Here, a supramolecular hydrogel-based, sol-gel transition electrolyte composed of thermotropic polymer Pluronic F-127 and α-CD additive is designed to afford dynamically adaptive contact between electrode and electrolyte. This in situ resetting strategy renders stable electrode-electrolyte interfaces and inhibits dendrite growth (Figure 1a). The SGTE formed by host-guest interactions between α-CD and polyethylene oxide (PEO) blocks of Pluronic exhibits excellent resetting ability and electrochemical performances. Due to the compatibility of Pluronic/α-CD with various electrolyte salts and high-concentration electrolytes, SGTEs based on $ZnSO_4$, $Zn(CF_3SO_3)_2$, and $ZnCl_2$ were further assembled into flexible Zn/MnO_2, Zn/V_6O_{13}, and Zn/PANI batteries, respectively. The resulting Zn/V_6O_{13} battery delivered a high specific capacity (413 $mAh\,g^{-1}$ at 0.1 $A\,g^{-1}$) and stable cyclability (81 % capacity retention after 500 cycles at 0.5 $A\,g^{-1}$).

The SGTE was facilely fabricated by stepwise dissolving Pluronic F-127 (polymer skeleton) and α-CD (cross-linking agent) in an ice water bath (Figure S1). As a non-ionic triblock copolymer with thermal gelation ability, Pluronic is polymorphic (PEO as the hydrophilic block and polypropylene oxide (PPO) as the hydrophobic block) in polar solvents such as water (Figure S2).[10] The self-assembly of hydrophobicity blocks is the driving force of Pluronic gelation. To improve the compatibility of Pluronic with higher salt concentration, α-CD with a hydrophilic outer surface and hydrophobic inner cavity was introduced to our gel electrolyte. α-CD was chosen due to its unique cavity

[*] P. Li,[+] Dr. M. Liao,[+] Dr. S. Cui, J. Li, Dr. L. Ye, Y. Yang, C. Wang, Prof. B. Wang, Prof. H. Peng
State Key Laboratory of Molecular Engineering of Polymers, Department of Macromolecular Science, and Laboratory of Advanced Materials, Fudan University
Shanghai 200438 (P. R. China)
E-mail: wangbingjie@fudan.edu.cn
penghs@fudan.edu.cn

[+] These authors contributed equally to this work.

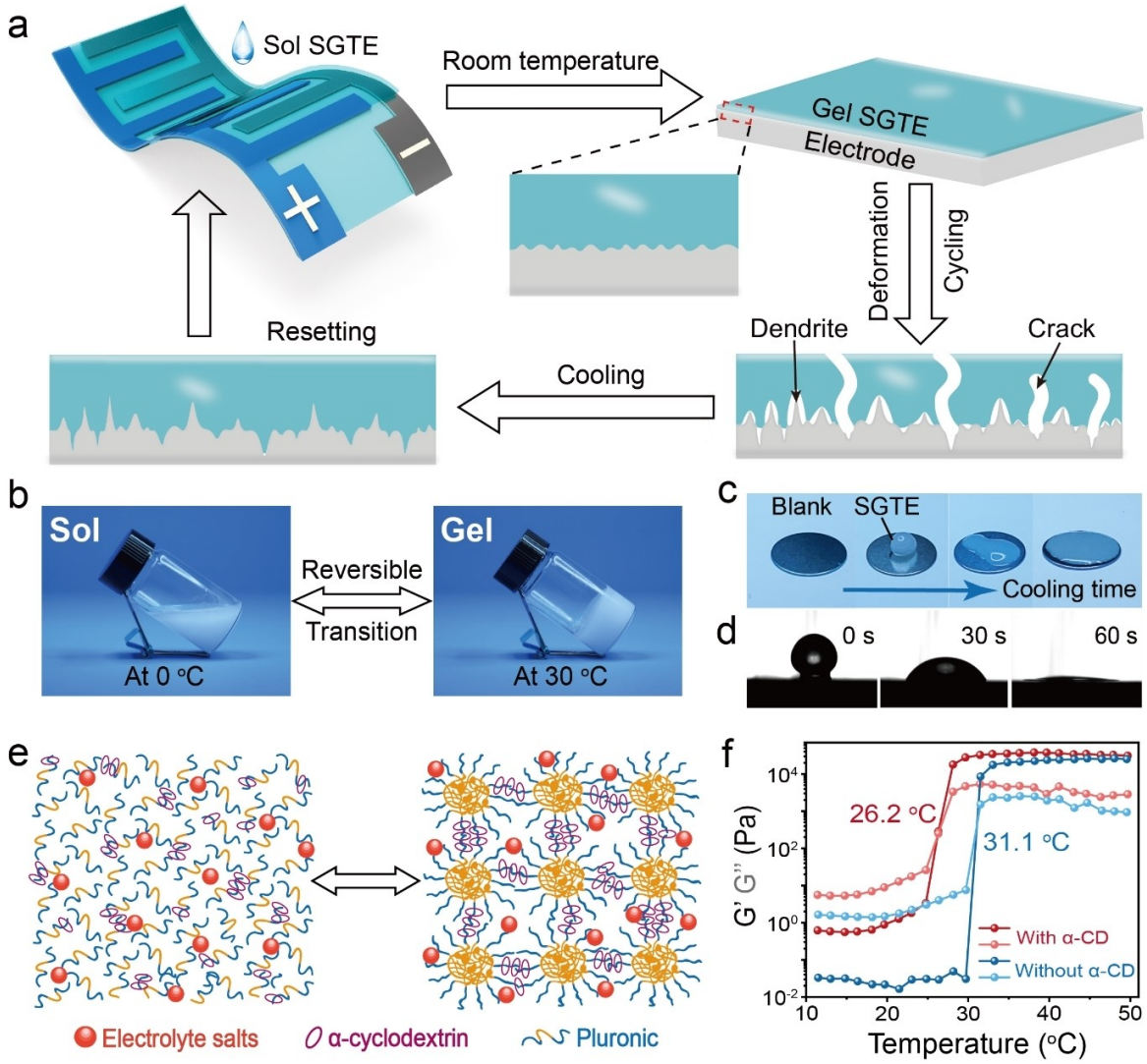

Figure 1. a) Schematic of SGTE for the dynamic resetting of the damaged electrode-electrolyte interface in a flexible battery. b) Sol-gel transition images of 1 M $Zn(CF_3SO_3)_2$ SGTE. c) Rapid wetting behavior of SGTE on a frozen metal electrode surface and d) corresponding contact angle changes over time. e) The sol-gel transition process of SGTE with α-CD at a higher electrolyte salt concentration. f) Rheological analysis of SGTE with and without α-CD containing 1 M $Zn(CF_3SO_3)_2$. The gelation temperature is defined as the crossover point of G′ and G″.

size (≈4.5 Å, compared with >7 Å for β-CD and γ-CD) that could selectively interact with PEO blocks, form stabilized pseudopolyrotaxane structure, and thus lower the sol-gel transition temperature in solutions.[11] Specifically, driven by the hydrophobic and non-covalent interactions between host and guest, α-CD could spontaneously self-assemble with PEO blocks to form pseudopolyrotaxane with enhanced solubility, thermo-sensitivity, and structural stability (Figure S3).[12] The as-prepared SGTE behaved sol-gel transition at a triggering temperature of ≈26 °C (room temperature), i.e., gelation when temperature surpasses 26 °C and converses to flowable sol upon cooling. This process was temperature-sensitive and highly reversible (Figure 1b). At room temperature, SGTE exhibited a uniform gel without phase separation, suggesting that there were fewer crystalline microdomains and beneficial to ion transport. When the temperature was decreased, SGTE transformed to sol with good fluidity. Due to the amphiphilic properties of Pluronic/α-CD, as-prepared SGTEs can infiltrate multiple electrodes rapidly. When SGTE was dropped onto a frozen metal electrode, unlike traditional liquid electrolytes, it could transform from a gel with large viscosity to a sol-like liquid, then spread quickly and wet the entire electrode surface (Figures 1c, d and S4), indicating the feasibility of dynamically resetting electrode-electrolyte interface.

The SGTE demonstrated decreased transparency upon increasing α-CD content (Figure S5) due to the assembled pseudopolyrotaxane via supramolecular interactions. Different from the pure Pluronic system, the gelation of SGTE

relied on both micellization of PPO in Pluronic and the inclusion of complexation between α-CD and PEO. A synthetic mechanism was proposed in Figure 1e, where PEO blocks were accessible to α-CD for the formation of pseudopolyrotaxane and partial crystallization, thus introducing new physical cross-linking points to form a network even at high electrolyte salt concentrations. Therefore, the sol-gel transition temperature of SGTE was optimized to room temperature considering the usage scenarios of flexible batteries (Figure S6). In addition to $ZnSO_4$ SGTE, several other salts with strong precipitation tendencies were selected according to the Hofmeister series, and their solubilities had been significantly improved in the polymer solution with α-CD added (Figure S7). The rheological analysis further confirmed that the gelation temperature (defined as the temperature where elastic modulus G′ is equal to viscous modulus G″) of SGTE with 1 M $Zn(CF_3SO_3)_2$ decreased from 31.1 to 26.2 °C with 12.5 % (w/w) α-CD addition (Figure 1f).

Characteristic X-ray diffraction peak at 19.4° indicated the channel-type structure of crystalline in SGTE. It verified the inner interactions between Pluronic and α-CD (Figure S8).[12,13] ^{1}H nuclear magnetic resonance spectra further proved that α-CD successfully self-assembled with PEO (Figure S9) by supramolecular interactions.[13] Pluronic@α-CD hydrogel exhibited porous structures in contrast to the dense morphology of pure Pluronic (Figure S10). This contributed to the accessibility of electrolytes for rapid ion transport and thus improved ionic conductivity.[14] The thermogravimetric analyzer was further applied to evaluate the thermostability, and SGTE with α-CD showed lower weight loss than that without α-CD (Figure S11). This increased thermostability could be attributed to the supramolecular interactions between host and guest in pseudopolyrotaxane.[15] By optimizing the ratio of Pluronic/α-CD/water, we could effectively adjust the sol-gel transition temperature and decrease the gelation temperature by increasing Pluronic/α-CD content (Figure S12). Due to the compatibility of Pluronic/α-CD with various electrolyte salts, SGTEs containing $ZnSO_4$, $Zn(CF_3SO_3)_2$, and $ZnCl_2$ were successfully prepared, all of which kept the gel state at room temperature, remained uniform without apparent phase separation even after dissolving 3 M $ZnCl_2$ and exhibited highly reversible sol-gel transition behavior (Figures 1f, S13, and S14).

Electrochemical tests were conducted to evaluate the performances of SGTE in batteries. Due to the stable structure of pseudopolyrotaxane, SGTE demonstrated an enlarger voltage window of up to 2.53 V compared to the corresponding liquid electrolyte (2.25 V) (Figure S15), indicating the supramolecular skeleton's stability and wide compatibility with various battery systems. Benefitting from the high electrolyte salt concentration and porous structure of SGTE, Nyquist impedance plots showed high ionic conductivities under various states or temperatures (Figure S16). Impressively, $ZnCl_2$ SGTE exhibited a high ionic conductivity of up to 58.3 mS cm^{-1} at 30 °C. Besides, Zn deposition/dissolution behavior in SGTE was similar to that in the corresponding liquid electrolyte (Figure S17), demonstrating the feasibility of SGTE as electrolytes for aqueous zinc batteries.

As is known, the dendrite growth in metallic anodes causes drastic volume changes and voids between the electrode and gel electrolyte. The locally increased current density would further aggravate the growth of dendrites and even lead to short circuits.[16] After certain cycles, SGTE-based batteries could be placed at 0 °C through a gel-sol transition to allow electrolytes to re-infiltrate and make seamless contact with the metallic anode, thus repairing uneven interface to extend the cycling lifespan. Zn||Zn symmetric cells were assembled with SGTE containing 1 M $Zn(CF_3SO_3)_2$ or liquid electrolyte to verify the resetting capability of the interface between the Zn anode and gel electrolyte. After cycling for 240 hours, the charge/discharge voltage of SGTE reset by sol-gel transition could be further maintained for over 360 hours without obviously increased overpotentials (Figure 2a). Benefited from the resetting procedure, this enhanced cycling lifespan outperformed that of the symmetric cell based on liquid electrolyte (Figure 2b) and SGTE without resetting process (Figure S18). The cell with liquid electrolyte had a short circuit and recovered from time to time, which was related to the dynamic short circuit connection, and the potential could be recovered once it was dissolved.[17] Even after cycling for 120 hours at 2 mA cm^{-2} and 2 mAh cm^{-2}, the cell can still operate for 280 hours after a resetting process. In comparison, the cell with liquid electrolyte experienced a sudden short circuit after 154 hours (Figure S19).

To study the influence of SGTE via resetting on Zn anodes, the morphology after cycling was investigated by scanning electron microscopy. After operating at 1 mA cm^{-2} and 1 mAh cm^{-2} for 50 cycles, the cell with SGTE was placed at 0 °C to transform the gel into a sol, then placed at room temperature to complete a sol-gel transition and continued cycling for 50 cycles. The cell with 1 M $Zn(CF_3SO_3)_2$ liquid electrolyte was directly stripped/plated for 100 cycles. A relatively uniform surface with crackle polymer coating was detected for SGTE via reset (Figures 2c and d). In sharp contrast, a typical uneven and dendritic surface was noted for liquid electrolytes without resetting (Figures 2e and f). The electrode before and after cycling was further analyzed by X-ray diffraction. Compared with few changes of Zn foil cycled with SGTE, more additional peaks appeared with liquid electrolyte due to the formation of by-products caused by Zn corrosion and other parasitic reactions (Figure S20).[18] These results indicated that this simple sol-gel transition strategy could effectively repair the damaged anode-electrolyte interface and prolong the battery lifespan.

SGTE can form a conformal contact with the Zn anode via in situ sol-gel transition during battery assembly (Figures S21 and S22). Note that the battery with SGTE could be stably operated at both 0 and 30 °C (Figure S23), implying this interface resetting process could be carried out without affecting the routine operation of batteries. The larger overpotential at the sol state was attributed to relatively slower electrode reaction kinetics at low temperatures.[19] To further verify the stable electrode-electrolyte interface formed by sol-gel transition, the long-

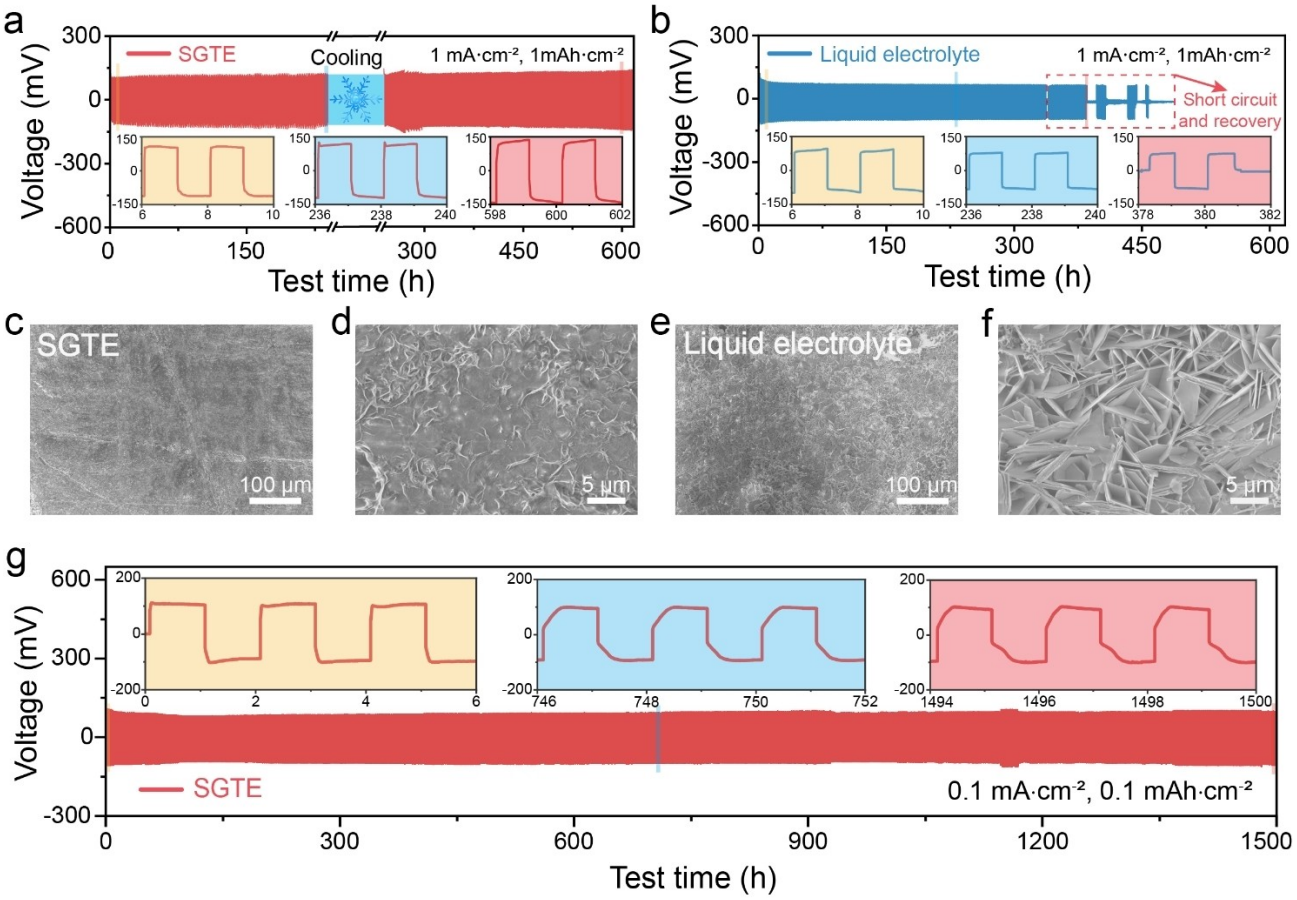

Figure 2. a), b) Overpotential variation trend of Zn||Zn symmetric cells based on (a) SGTE with and (b) liquid electrolyte without resetting process. c)–f) Low and high magnification scanning electron microscopy images of Zn anode morphologies after plating/stripping 100 cycles at 1 mA cm^{-2} and 1 mAh cm^{-2} based on (c, d) SGTE and (e, f) liquid electrolyte. g) Long-time cycling performance of Zn||Zn symmetric cells at 0.1 mA cm^{-2} and 0.1 mAh cm^{-2}, insets are selected potential profiles at the different stages.

time cycling stability of Zn||Zn symmetric cells was tested at 0.1 mA cm^{-2} for 0.1 mAh cm^{-2} (Figure 2g). The overpotential remained stable during 1500 hours and decreased from 107 mV at the 1st cycle to 98 mV at the 750th cycle, demonstrating an ultra-stable interface and uniform ion transport over a long duration. Note that the evolution of voltage profiles upon cycling was due to the formation of highly active porous Zn on the surface of bulk Zn.[20] Moreover, upon continuous cycling under increasing current densities from 0.1 to 2.0 mA cm^{-2}, stable voltage-time curves were obtained with marginally increased overpotentials (Figure S24).

For flexible batteries with conventional gel electrolytes, only the outside layer of electrode materials can well contact gel electrolytes, thus leading to a low specific capacity.[21] The electrode and electrolyte interface will be damaged under deformations and the defects will be further aggravated with deeper cycling, which can eventually cause capacity loss and even battery collapse. The SGTE took on a gel state at room temperature, which was conducive to battery integration and improvement of flexibility. When flexible batteries with SGTE had internal interface defects due to mechanical deformations, they could be stored at 0 °C to convert gel into a sol to re-wet the interface between functional components and restore electrochemical performances. Interdigitated flexible batteries were further fabricated by screen printing and in situ coating of sol SGTE (Figures S25–S27). The thicknesses with electrodes printed and SGTE coated were only 182 and 421 μm, respectively (Figure S28). Afterward, the interface resetting process at different times after intensive folding was recorded by scanning electron microscopy. It was noted that the electrode interface had obvious cracks after intensive folding (Figures 3a, b). Just by placing the battery at 0 °C, we found SGTE transformed into a flowable sol and the damaged interface could be effectively repaired within 5 minutes (Figures 3c–e). This easy-handling in situ gel-sol transition made use of the characteristics of liquid electrolytes with low viscosity, which made flexible batteries with fewer defects for ionic transport and gave full access to active materials. The comparison of cyclic voltammetry and electrochemical impedance spectroscopy curves before and after the sol-gel transition showed high coincidence, indicating good resetting ability (Figures 3f and g).

When a flexible battery based on SGTE was folded in half several times, the cracks between the electrode and

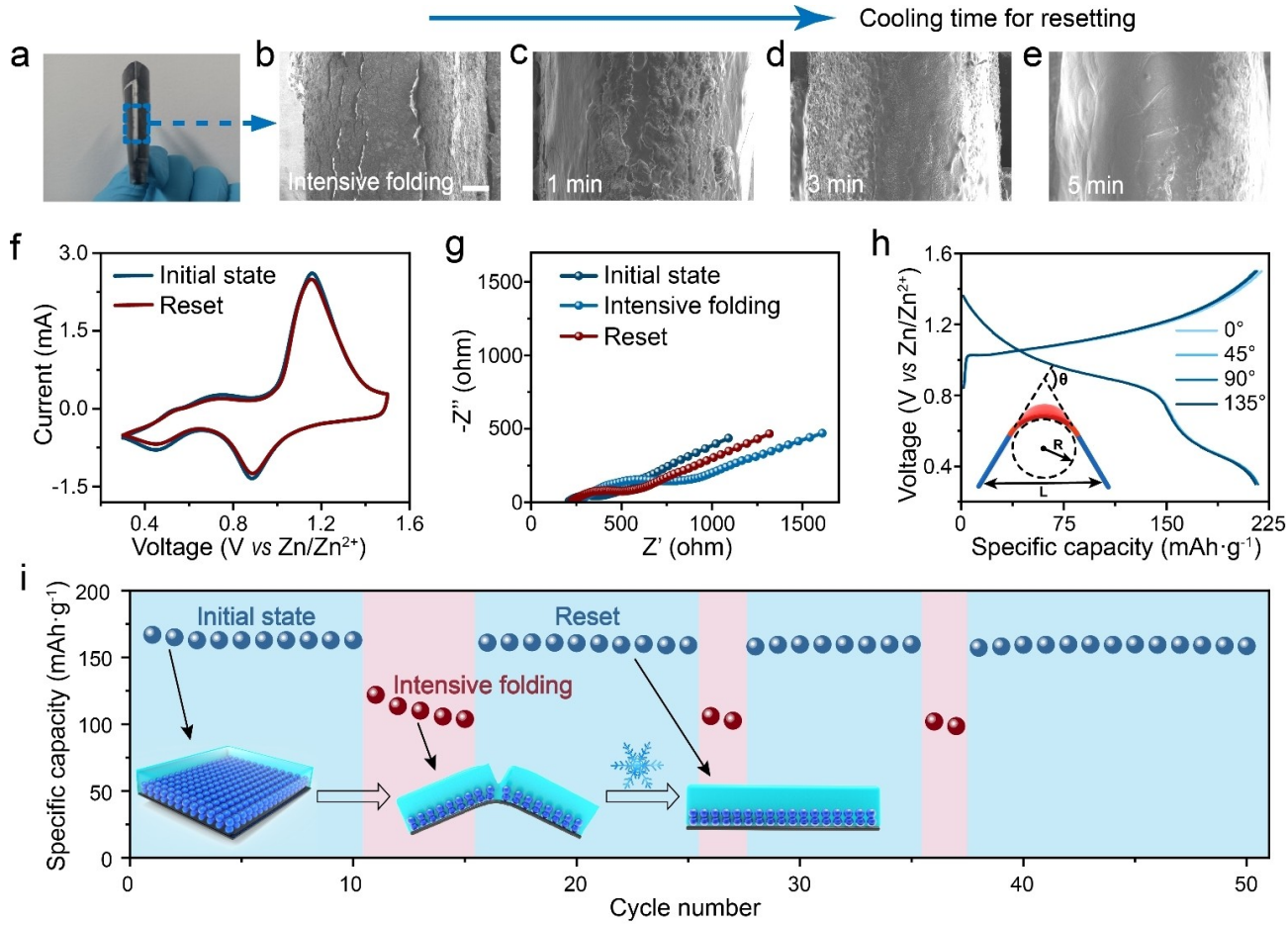

Figure 3. a) Photograph of a flexible battery after intensive folding. b) Top-viewed scanning electron microscopy images of the broken flexible electrode with SGTE due to intensive folding and c)–e) the resetting area after 1, 3, and 5 minutes at 0 °C. f) Cyclic voltammetry curves and g) electrochemical impedance spectra of flexible Zn/SGTE/V_6O_{13} battery at initial, intensive folding, and after resetting state. h) Galvanostatic charge–discharge curves of flexible Zn/SGTE/V_6O_{13} battery at increasing bending angles ranging from 0 to 135° at 0.5 A g^{-1}. i) Cycling performance of flexible Zn/SGTE/V_6O_{13} battery in various states at 1.0 A g^{-1}. Scale bar, 100 μm in (b)–(e).

electrolyte interface would cause obvious capacity loss due to reduced utilization of active materials, and the specific capacity (based on the mass loading of V_6O_{13}) directly dropped from 163 to 104 mAh g^{-1} (11^{th} to 15^{th} cycles) (Figures 3i and S29). Afterward, the battery was stored at 0 °C for 3 minutes and the sol transformed from the gel was adequately re-infiltrated into active materials. Upon recovering to room temperature, a quasi-solid-state battery with enhanced utilization of active materials was achieved and then subjected to charge/discharge cycles. Note that the specific capacity with SGTE was recovered significantly with almost no gap from the initial state. Moreover, this dynamic resetting process was reversible and repeatable. The capacity retention could still maintain 95 % even after three intensive folding/resetting processes, indicating that SGTE could effectively achieve the dynamic resetting of the damaged electrode-electrolyte interface. This strategy avoids the need to destroy the encapsulation layer, achieved an extended battery lifespan, and reduces electronic waste. In addition, owing to the dynamic flow properties of the sol to accommodate the electrode surface, the assembled flexible battery via in situ sol-gel transition also had a stable cathode-electrolyte interface (Figure S30). The device length (L) and bending radius (R) were kept constants (R: 1 cm; L: 4 cm), and the bending angle (θ) was changed from 0 to 135° to manifest the bending state.[22] The capacity retention was more than 90 % even at 135° (Figure 3h) and was only slightly attenuated to 95.7 % after it was continuously bent every 100 times ($\theta = 135°$) through resetting treatments (Figure S31), demonstrating a stable interface and excellent flexibility. Besides, the open-circuit voltage (OCV) changes of the flexible Zn/SGTE/V_6O_{13} battery were recorded by a multimeter, and it kept stable under bending and rapidly decreased to 1.277 V under intensive folding, but the OCV recovered to 1.328 V again after 0 °C treatment, further proving the stable interface and excellent resetting ability (Figure S32).

To prove the feasibility of SGTE in multiple aqueous battery systems, flexible Zn/MnO_2, Zn/V_6O_{13}, and Zn/PANI batteries based on corresponding SGTEs were fabricated via screen printing (Figures 4a–c). The overlapped cyclic voltammetry and galvanostatic charge/discharge curves in the

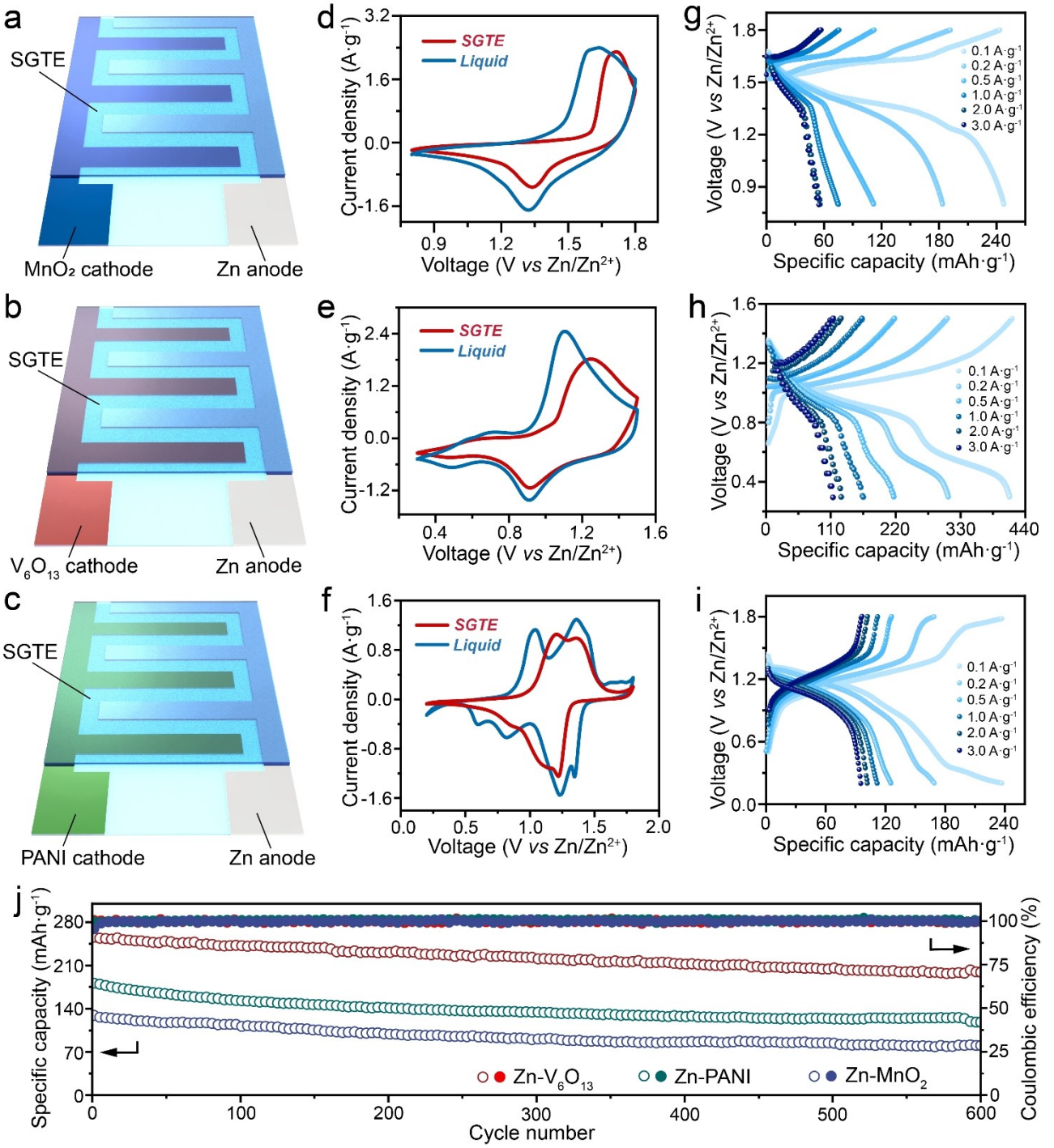

Figure 4. a)–c) Schematic illustration of flexible Zn/MnO_2, Zn/V_6O_{13}, and Zn/PANI batteries based on 0.6 M $ZnSO_4$ + 0.05 M $MnSO_4$, 1 M $Zn(CF_3SO_3)_2$, and 3 M $ZnCl_2$ SGTEs, respectively. d)–f) Cyclic voltammetry curves of liquid and SGTE-based flexible Zn/MnO_2, Zn/V_6O_{13}, and Zn/PANI batteries. g)–i) Galvanostatic charge–discharge profiles of flexible Zn/MnO_2, Zn/V_6O_{13}, and Zn/PANI batteries with SGTEs at increasing current densities from 0.1 to 3.0 A g^{-1}. j) Cycling performance of flexible Zn/V_6O_{13}, Zn/PANI, and Zn/MnO_2 batteries with SGTEs at 0.5 A g^{-1}.

first three cycles and the wide temperature range of 20 to 70 °C demonstrated a highly reversible Zn^{2+} (de)intercalation reaction at the initial stage and excellent environmental adaptability (Figures S33 and S34). The redox peaks in cyclic voltammetry curves based on SGTE presented high similarity to liquid electrolytes and agreed well with the voltage plateaus of galvanostatic charge/discharge profiles, indicating that the similar energy storage mechanism of SGTE with the liquid electrolyte (Figures 4d–f). The larger polarization and smaller peak current of SGTE could be attributed to the higher viscosity and lower mobility of Zn^{2+}.[23] Besides, the charge/discharge profiles at

various current densities presented similar shapes (Figures 4g–i) and the capacity could immediately recover with the reversal of applied current densities ranging from 0.1 to 3 $A g^{-1}$ for over 60 cycles (Figure S35), demonstrating fast charge transfer kinetics. Such facilitated kinetics could be attributed to a surface-controlled capacity contribution of up to 85.7 % from cyclic voltammetry studies (Figure S36 and Note S1). Due to the stable electrode-electrolyte interfaces by in situ sol-gel transition, the specific capacities of flexible Zn/V_6O_{13}, Zn/MnO_2, and Zn/PANI batteries could still maintain at 199, 118, and 80.3 $mAh g^{-1}$ at 0.5 $A g^{-1}$ over 600 cycles, respectively (Figure 4j). Note that besides flexible Zn-based batteries, our SGTE also showed effectiveness upon its utilization in flexible hybrid supercapacitors (Figure S37). These results indicated that our SGTE could be utilized for a spectrum of inorganic and polymer electrode materials for zinc batteries based on similar energy-storing mechanisms.[24] Even operating at 1.0 $A g^{-1}$ for 1000 cycles, the specific capacity only showed limited decay (Figure S38). The SGTE-based flexible battery also showed advantageous performances compared with previous reports (Table S1).[25] As an application demonstration, a temperature and humidity meter could be effectively powered by one flexible $Zn/SGTE/MnO_2$ battery while a light-emitting diode can be illuminated by two batteries in series (Figure S39).

In conclusion, a facile and general strategy to achieve stable electrode-electrolyte interfaces for durable, flexible batteries had been developed by designing supramolecular hydrogel-based, dynamically resettable SGTEs. The transition temperature was flexibly adjustable and the transition process was highly reversible. Due to the compatibility of Pluronic/α-CD with different types and high concentrations of electrolyte salts, three representative SGTEs were obtained and $ZnCl_2$ SGTE exhibited high ionic conductivity of 58.3 $mS cm^{-1}$. Flexible batteries with SGTEs had stable electrode-electrolyte interfaces owing to the in situ sol-gel transition and the damaged interface could be effectively repaired via simply cooling treatment. The $Zn/SGTE/V_6O_{13}$ battery delivered a high specific capacity of 413 $mAh g^{-1}$ and stable cyclability up to 1000 cycles. This work provides a new strategy to fabricate all-in-one flexible batteries with dynamic interface resetting ability, contributing to the development of wearable electronics.

Acknowledgements

This work was supported by STCSM (21511104900, 20JC1414902) and NSFC (52222310).

Conflict of Interest

The authors declare no conflict of interest.

Data Availability Statement

The data that support the findings of this study are available from the corresponding author upon reasonable request.

Keywords: Electrode-Electrolyte Interface · Flexible Battery · Sol-Gel Transition · Wearable Electronics

[1] F. Mo, G. Liang, Z. Huang, H. Li, D. Wang, C. Zhi, *Adv. Mater.* **2020**, *32*, 1902151.
[2] a) Y. Zhang, F. Wan, S. Huang, S. Wang, Z. Niu, J. Chen, *Nat. Commun.* **2020**, *11*, 2199; b) L. E. Blanc, D. Kundu, L. F. Nazar, *Joule* **2020**, *4*, 771–799; c) M. Liao, J. Wang, L. Ye, H. Sun, P. Li, C. Wang, C. Tang, X. Cheng, B. Wang, H. Peng, *J. Mater. Chem. A* **2021**, *9*, 6811–6818.
[3] a) P. Li, M. Liao, J. Li, L. Ye, X. Cheng, B. Wang, H. Peng, *Small Struct.* **2022**, *3*, 2200058; b) L. Li, Q. Zhang, B. He, R. Pan, Z. Wang, M. Chen, Z. Wang, K. Yin, Y. Yao, L. Wei, L. Sun, *Adv. Mater.* **2022**, *34*, 2104327.
[4] a) M. Liao, C. Wang, Y. Hong, Y. Zhang, X. Cheng, H. Sun, X. Huang, L. Ye, J. Wu, X. Shi, X. Kang, X. Zhou, J. Wang, P. Li, X. Sun, P. Chen, B. Wang, Y. Wang, Y. Xia, Y. Cheng, H. Peng, *Nat. Nanotechnol.* **2022**, *17*, 372–377; b) L. Ma, S. Chen, X. Li, A. Chen, B. Dong, C. Zhi, *Angew. Chem. Int. Ed.* **2020**, *59*, 23836–23844; *Angew. Chem.* **2020**, *132*, 24044–24052.
[5] a) Q. Yang, Q. Li, Z. Liu, D. Wang, Y. Guo, X. Li, Y. Tang, H. Li, B. Dong, C. Zhi, *Adv. Mater.* **2020**, *32*, 2001854; b) F. Xie, H. Li, X. Wang, X. Zhi, D. Chao, K. Davey, S. Qiao, *Adv. Energy Mater.* **2021**, *11*, 2003419; c) Z. Shen, Z. Tang, C. Li, L. Luo, J. Pu, Z. Wen, Y. Liu, Y. Ji, J. Xie, L. Wang, Y. Yao, G. Hong, *Adv. Energy Mater.* **2021**, *11*, 2102055.
[6] Y. Cho, C. Hwang, D. Cheong, Y. Kim, H. Song, *Adv. Mater.* **2019**, *31*, 1970144.
[7] K. Leng, G. Li, J. Guo, X. Zhang, A. Wang, X. Liu, J. Luo, *Adv. Funct. Mater.* **2020**, *30*, 2001317.
[8] Y. Huang, J. Liu, J. Wang, M. Hu, F. Mo, G. Liang, C. Zhi, *Angew. Chem. Int. Ed.* **2018**, *57*, 9810–9813; *Angew. Chem.* **2018**, *130*, 9958–9961.
[9] a) X. Xiao, X. Xiao, Y. Zhou, X. Zhao, G. Chen, Z. Liu, Z. Wang, C. Lu, M. Hu, A. Nashalian, S. Shen, K. Xie, W. Yang, Y. Gong, W. Ding, P. Servati, C. Han, S. X. Dou, W. Li, J. Chen, *Sci. Adv.* **2021**, *7*, eabl3742; b) F. Mo, H. Li, Z. Pei, G. Liang, L. Ma, Q. Yang, D. Wang, Y. Huang, C. Zhi, *Sci. Bull.* **2018**, *63*, 1077–1086.
[10] S. Soni, K. Fadadu, A. Gibaud, *Langmuir* **2012**, *28*, 751–756.
[11] a) K. Zhao, G. Fan, J. Liu, F. Liu, J. Li, X. Zhou, Y. Ni, M. Yu, Y. Zhang, H. Su, Q. Liu, F. Cheng, *J. Am. Chem. Soc.* **2022**, *144*, 11129–11137; b) C. Travelet, G. Schlatter, P. Hébraud, C. Brochon, A. Lapp, G. Hadziioannou, *Langmuir* **2009**, *25*, 8723–8734.
[12] J. Li, X. Li, Z. Zhou, X. Ni, K. Leong, *Macromolecules* **2001**, *34*, 7236–7237.
[13] C. Pradal, K. Jack, L. Grøndahl, J. CooperWhite, *Biomacromolecules* **2013**, *14*, 3780–3792.
[14] J. Wang, Q. Fang, L. Ye, A. Zhang, Z. Feng, *Soft Matter* **2020**, *16*, 5906–5909.
[15] H. Wei, H. Yu, A. Zhang, L. Sun, D. Hou, Z. Feng, *Macromolecules* **2005**, *38*, 8833–8839.
[16] T. C. Li, D. Fang, J. Zhang, M. E. Pam, Z. Y. Leong, J. Yu, X. L. Li, D. Yan, H. Y. Yang, *J. Mater. Chem. A* **2021**, *9*, 6013–6028.
[17] Q. Li, A. Chen, D. Wang, Z. Pei, C. Zhi, *Joule* **2022**, *6*, 273–279.
[18] N. Zhang, F. Cheng, Y. Liu, Q. Zhao, K. Lei, C. Chen, X. Liu, J. Chen, *J. Am. Chem. Soc.* **2016**, *138*, 12894–12901.

[19] M. Zhu, X. Wang, H. Tang, J. Wang, Q. Hao, L. Liu, Y. Li, K. Zhang, O. G. Schmidt, *Adv. Funct. Mater.* **2020**, *30*, 1907218.
[20] Q. Li, A. Chen, D. Wang, Y. Zhao, X. Wang, X. Jin, B. Xiong, C. Zhi, *Nat. Commun.* **2022**, *13*, 3699.
[21] L. Ma, S. Chen, C. Long, X. Li, Y. Zhao, Z. Liu, Z. Huang, B. Dong, J. A. Zapien, C. Zhi, *Adv. Energy Mater.* **2019**, *9*, 1902446.
[22] Q. Li, D. Wang, B. Yan, Y. Zhao, J. Fan, C. Zhi, *Angew. Chem. Int. Ed.* **2022**, *61*, e202202780; *Angew. Chem.* **2022**, *134*, e202202780.
[23] M. Chen, J. Chen, W. Zhou, X. Han, Y. Yao, C. Wong, *Adv. Mater.* **2021**, *33*, 2007559.
[24] Y. Zhang, L. Zhao, Y. Liang, X. Wang, Y. Yao, *eScience* **2022**, *2*, 110–115.
[25] B. Wu, Y. Mu, Z. Li, M. Li, L. Zeng, T. Zhao, *Chin. Chem. Lett.* **2023**, *34*, 107629.

Manuscript received: January 14, 2023
Accepted manuscript online: February 27, 2023
Version of record online: March 15, 2023